# On the Efficacy of the Wavelet Decomposition for High Frequency Vibration Analyses

S. Zhang and L. Cheng[¯]

*Department of Mechanical Engineering*
*The Hong Kong Polytechnic University*
*Hung Hom, Kowloon, Hong Kong SAR, P. R. China*
*Li.cheng@polyu.edu.hk*

**Abstract**

This paper reports the extraordinary ability of the wavelet decomposition for vibration analyses under the framework of Rayleigh-Ritz method. Using a beam as an example, Daubechies wavelet scale functions are used as admissible functions for decomposing the flexural displacement of the structure, along with the artificial springs at the boundary, to predict vibration of an Euler-Bernoulli beam in an extremely large frequency range. It is shown that the use of wavelet basis allows reaching very high frequencies, typically covering more than one thousand modes using conventional computational facility within the available numerical dynamics of the computers with no particular care needed for round-off errors. As a side benefit, the use of spring boundary also allows handling any elastic boundary conditions through a dynamic contribution in the Hamiltonian of the beam. The wavelet decomposed approach combines the flexibility of the global methods and the accuracy of local methods by inheriting the versatility of the Rayleigh-Ritz approach and the

[¯] Corresponding author, e-mail: li.cheng@polyu.edu.hk, phone: 852-2766 6769, fax: 852-2365 4703

superior fitting ability of the wavelets. Numerical results on both free and forced vibrations are given, in excellent agreement with predictions of classical methods.

## 1 Introduction

Vibration analyses of structures in the mid-to-high frequency range pose formidable technical changes to the existing simulation methods [1]. Particular problems arising are mainly twofold. First, wavelengths get shorter as the frequency increases, so that more structural details need to be considered in the model, leading to exorbitant computational cost. Second, due to the high sensitivity of the vibrational behavior to structural details and model parameters at higher frequencies, any inaccuracy in the model or round-off errors in numerical simulation will lead to erroneous results. In order to satisfy the demand for the vast amount of parametric and optimization studies in the preliminary design stage of structures, versatile and efficient simulation methods which can potentially cover a wide frequency spectrum is of paramount importance.

Among various so-called semi-analytical methods based on spatial discretization [2], Rayleigh-Ritz method with assumed admissible functions is probably the most popular and most studied one. It consists in approximating the unknown structural displacement through a linear combination of assumed global basis functions. The basis function should, *a priori*, satisfies the geometric boundary conditions, which can

be tactically avoided through the use of artificial spring along structural boundaries [2]. Based on the Hamilton's principle, the elastic boundary conditions are apprehended in the elastic energy term in the Hamiltonian of the structures, the extremalization of which can be achieved using Lagrange's equation. There is huge amount of literature on the topic, and typical applications can be found in Cheng and Lapointe [3] and Berry *et al*. [4]. The properties of the basis functions significantly affect the computational efficiency, stability and accuracy of the solution. Popular candidates are polynomials [3, 4] and their derivatives such as Jacobi polynomials [5], Legendre polynomials [6] or Chebyshev polynomials [7]. However, they all suffer from the ill-conditioned problem [8] at higher order. This is due to the mismatch of the high numerical dynamics of the polynomial coefficients and the limited numerical dynamics of the digital computers; which is unavoidable even for symbolic computing. It is reported that the highest polynomial order that could possibly be used is roughly 19, and 44 for symbolic case [8] for one dimensional structure. Using the rule of thumb that roughly one-third to half of the modes can be correctly predicted, only less than twenty modes can be, in principle, corrected calculated. Trigonometric functions [9] or combination of the trigonometric functions and lower-order polynomials [10, 11] are also possible choice. However, trigonometric functions suffer from potential convergence problems on the boundary [11]. To the best of our

knowledge, practically nothing in the open literature shows their efficiency in dealing with very high-order modes except for Beslin's work [8] in which natural modes of a plate were computed, roughly reaching what can be quantified as the mid-frequency range of the structure (880 natural frequencies within 1.5% of error in 2-D structure, roughly corresponding to 30 modes in 1D scenario).

Wavelets have been widely used in signal processing in various applications including sound and vibration. However, their efficacy in vibration simulations, especially as a global basis under the Rayleigh-Ritz framework, has never been explored up to now. Inspired by the appealing features of Daubechies wavelet scale functions in numerical approximation and our recent success in acoustic simulation using Galerkin formulation [12], this paper examines the use of the Daubechies wavelet scale functions as basis functions for vibration prediction under the general framework of Rayleigh-Ritz method. Daubechies wavelet scale functions have been shown to exhibit strong ability to express any square integrable functions in finite interval, high vanishing moments and orthogonality [13]. Using a beam example, it is shown that the proposed Wavelet Decomposed Rayleigh-Ritz method (WDRM) allows reaching very high frequencies without being restrained by the limited numerical dynamics of the computer with no particular care for round-off errors. While inheriting all the merits of Rayleigh-Ritz method, the proposed method

combines the flexibility of the global methods and the accuracy of the local methods [12]. For implementation, proper treatment should be made to evaluate the derivatives of Daubechies wavelet scale functions due to its strong oscillation and lack of closed-form expression.

It is shown in this paper that the Daubechies wavelet scale functions can be used as admissible functions in Rayleigh-Ritz method and exhibit remarkable features for the vibration analyses of beams with arbitrary elastic boundaries. The limitations of the method using conventional admissible functions can be overcome since the wavelet basis can significantly reduce the round-off errors to avoid the ill-conditioned problems generally encountered. As a result, using normal computation facility, over one thousands of natural modes can be accurately predicted with an error caped at 1%, outperforming any other basis functions reported in the literature under the frame of Rayleigh-Ritz method. Calculation cases are chosen for demonstrating the accuracy of the proposed Wavelet-based approach. Results on natural modes (from low to high frequencies) were provided. Although individual modes are less important at extra high frequencies, they are useful parameters which allow comparisons with existing analytical solutions. We also calculate the forced vibration responses which do not require the prior calculations of the modes. Results on both free and forced vibrations allow demonstrating that the proposed method is capable of dealing with typical

vibration problems in a very wide frequency range, especially at high frequencies, where most of existing methods fail.

The paper is organized as follows. Section 2 is devoted to the theoretical modeling. The formulation for the beam vibrations, detailed in Sec. 2.1, is based on the Hamilton's principle; the elastic boundary conditions appear through a dynamic contribution in the Hamiltonian of the beam. The extremalization of the Hamiltonian is achieved using Lagrange's equation. Numerical results are presented and discussed in Sec.3. The eigen-frequency and mode shape are shown. Comparisons with predictions by classic methods are made both in free-free and pinned-pinned cases. Then the forced vibration response is presented and compared with analytical solution for a large frequency band involving thousands of modes under pinned-pinned boundary conditions.

## 2 Method

### 2.1 Beam model

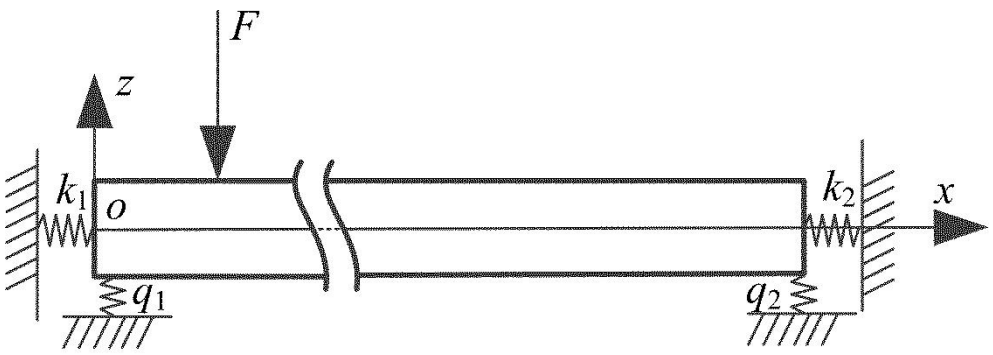


Fig.1 Euler-Bernoulli beam model.

As shown in Fig.1, the investigated structure is a uniform Euler-Bernoulli beam. The mounting conditions are simulated by a set of artificial translational and rotational springs ($k_i$ in N/m for translation and $c_i$ in N/rad). The use of springs allows the representation of a wide variety of boundary conditions by adjusting the stiffness values of the springs [3]. For example, simply supported boundaries can be obtained by using a sufficiently large $k_i$ and a zero $c_i$. For the completeness of the paper, the classical Rayleigh-Ritz procedure is briefly recalled.

The flexural displacement $w(x, t)$ of the beam can be expanded as

$$w(x,t) = \sum_i a_i(t) f_i(x) \tag{1}$$

where $f_i(x)$ are the assumed admissible functions and $a_i(t)$ unknowns to be determined.

The Lagrange's equations can then be applied to find the stationary state of the system with $a_i(t)$ as generalized coordinates:

$$\frac{d}{dt}\left(\frac{\partial L}{\partial \dot{a}_i(t)}\right) - \frac{L}{a_i(t)} = 0 \quad , (i = 0,1,2,\mathrm{L}\ ,n) \tag{2}$$

where $L$ is the Lagrangian of the system expressed as

$$L = E_k - E_p + W \tag{3}$$

where the kinetic energy $E_k$, potential energy, $E_p$ and the work, $W$, done by the external excitation force $f(t)$ write:

$$E_k = \frac{1}{2} rBh \int_0^l \left( \frac{\partial w}{\partial t} \right)^2 dx \tag{4}$$

$$\begin{aligned} E_p = {} & \frac{1}{2} \int_0^l EI \left( \frac{\partial^2 w}{\partial x^2} \right)^2 dx + \frac{1}{2} k_1 w(0,t)^2 + \frac{1}{2} q_1 \left( \frac{\partial w(0,t)}{\partial x} \right)^2 \\ & + \frac{1}{2} k_2 w(l,t)^2 + \frac{1}{2} q_2 \left( \frac{\partial w(l,t)}{\partial x} \right)^2 \end{aligned} \tag{5}$$

$$W = f(t) w(x_F, t) \tag{6}$$

where $l$ is the length of the beam; $\rho$ the density of the material; $B$ and $h$ the width and height of the cross section area, respectively; $x_F$ the location of the excitation force.

Substituting Eqs. to into Eq.(3) yields the following linear equations in matrix form

$$[M]\{\ddot{a}(t)\} + [K]\{a(t)\} = \{f(t)\} \tag{7}$$

where $[M]$ and $[K]$ are, respectively, the mass matrix and stiffness matrix. In a harmonic regime,

$$\{f(t)\} = \{F\} e^{j\omega t} \tag{8}$$

$$\{a(t)\} = \{A\} e^{j\omega t} \tag{9}$$

Eq. can be rewritten as

$$[[K] - \omega^2 [M]]\{A\} = \{F\} \tag{10}$$

the solution of which gives the natural frequencies and the corresponding mode shapes.

Expressions for $[M]$ and $[K]$ are

$$M_{i,j} = rBh \int f_i(x) f_j(x)\, dx \tag{11}$$

$$K_{i,j} = \frac{EBh^3}{12} \int f_i''(x) f_j''(x)\, dx + k_1 f_i(0) f_j(0) + q_1 f_i(0) f_j(0) + k_2 f_i(l) f_j(l) + q_2 f_i(l) f_j(l) \tag{12}$$

**2.2 Wavelet decomposition**

The mathematical theory on wavelet analysis is readily available. Details can be found in the references [13]. Here, we only focus on the idea of the decomposition into orthogonal functions of different scales and locations. The wavelet basis we choose is an ensemble of wavelet series with its members being represented as linear combinations of finite sets of scaled, translated, copies of the scaling function.

Daubechies wavelet is a family of compactly supported orthogonal wavelets including both highly localized and highly smooth members. Each wavelet member is governed by a set of $L$ (an even integer) coefficients $\{h_j: j=0,1,\ldots,L-1\}$ through two-scale relations

$$\varphi(x) = \sum_{j=0}^{L-1} h_j \varphi(2x - j) \tag{13}$$

and

$$\psi(x) = \sum_{j=2-L}^{1} (-1)^j h_{1-j} \varphi(2x - j) \tag{14}$$

where $\varphi(x)$ and $\psi(x)$ are the scaling function and mother wavelet, respectively. The fundamental support of the scaling function $\varphi(x)$ is the interval [0, $L$-1] while that of the corresponding wavelet $\varphi(x)$ is in the interval [1-$L$/2, $L$/2]. The coefficients $h_j$ in

the two-scale relation are the wavelet filter coefficients. Values of these coefficients can be found in the literature. The scaling function $j(x)$ has the following properties:

$$\int_{-\infty}^{\infty} x^k y(x)dx = 0, \quad k = 0,1,\ldots,L/2-1 \tag{15}$$

Note that the property expressed above is equivalent to that the elements of the set {1, $x$,…, $x^{L/2-1}$} are a linear combination of $j(x-k)$, which is a integer translate of $j(x)$. So the scaling function $j(x)$ can be used to approximate a function within an interval [14].

The assumed admissible functions is therefore defined as

$$f_i(x) = 2^{m/2} j(2^m x - i) \tag{16}$$

where $m$ is the resolution of wavelet scale functions.

Eq. requires the derivatives of wavelet bases to be evaluated. Since the derivatives of compactly supported wavelets are highly oscillatory, it is unfeasible and numerically unstable to compute the derivatives numerically. In order to overcome this problem, dedicated algorithms called recursion method have been derived for the exact evaluation of derivatives [14, 15].

The $n$th derivative of the scaling function, denoted by $j^{(n)}(x)$ writes

$$j^{(n)}(x) = \frac{d^n j(x)}{dx^n} = \frac{d}{dx} j^{(n-1)}(x), \qquad j^{(0)}(x) = j(x) \tag{17}$$

Substituting the two-scale relationship Eq. into the above equation yields

$$j^{(n)}(x) = 2^n \sum_{k=0}^{L-1} h_k j^{(n)}(2x-k)dx \tag{18}$$

Eq. is the two-scale relationship for $j^{(n)}(x)$, which can be used to compute $j^{(n)}(x)$ at all dyadic points $x = k/2^j$, $j = 1,2,\mathrm{K}$, ¥ , provided that the values of $j^{(n)}(k)$, $k = 1,2,\mathrm{K}\ L-2$ are given. The above can be referred to as recursive procedure.

To get $j^{(n)}(x)$ at integer points, we substitute $x = 1,2,\mathrm{K}, L-2$ into Eq., resulting in the following homogeneous linear system

$$(\mathrm{H} - 2^{-n}\mathrm{I})\boldsymbol{\Phi} = 0 \tag{19}$$

where

$$\boldsymbol{\Phi} = \begin{bmatrix} j^{(n)}(1) & j^{(n)}(2) & \mathrm{L} & j^{(n)}(L-2) \end{bmatrix}^{\mathrm{T}} \tag{20}$$

$\mathrm{H}$ is a $(L-2)\times(L-2)$ matrix

$$\mathrm{H} = \begin{bmatrix} \\ \\ \\ \end{bmatrix}_{s-t\ 1\le s,t\le L-2} \tag{21}$$

with $s$ being the row index and $t$ the column index. Eq. indicates that the unknown vector $\mathrm{F}$ is the eigenvector of the matrix $\mathrm{H}$ corresponding to the eigenvalues $2^{-n}$. The values $j^{(n)}(x)$ at integer points, $x = 1,2,\mathrm{K}, L-2$, can be determined after getting the eigenvector of $\mathrm{H}$ which corresponds to the eigenvalues $2^{-n}$, and then be normalized as

$$\sum_{k=1}^{L-2} (-k)^n j^{(n)}(k) = n! \tag{22}$$

Upon getting $j^{(n)}(x)$, Eq.(18) can be written as

$$j^{(n)}\left(\frac{k}{2^j}\right) = 2^n \sum_{l=0}^{L-1} h_l\, j^{(n)}\left(\frac{k}{2^{j-1}} - l\right) \tag{23}$$

The use of above equation and $j^{(n)}(x) = 0$ outside the support length ( $x \le 0$ and $x \ge L-1$ ) allows one to determine the values of $j^{(n)}(x)$ at all dyadic points $x = k/2^j, k = 1,2,\mathrm{K}\ ,2^j(L-1)-1$ and $j = 1,2,\mathrm{K}$ .

A comparison is made with the traditional numerical scheme based on finite difference method (FDM), expressed as

$$j'(x_0) \approx \frac{j(x_0+h)-j(x_0)}{h} \tag{24}$$

As shown in Fig. 2, the discrepancy of the 1st order derivatives of D6 wavelet scale function between recursive method and FDM are significant. Compared with the exact value calculated by recursive method at dyadic points, FDM has large errors. Therefore, the FDM cannot be directly used.

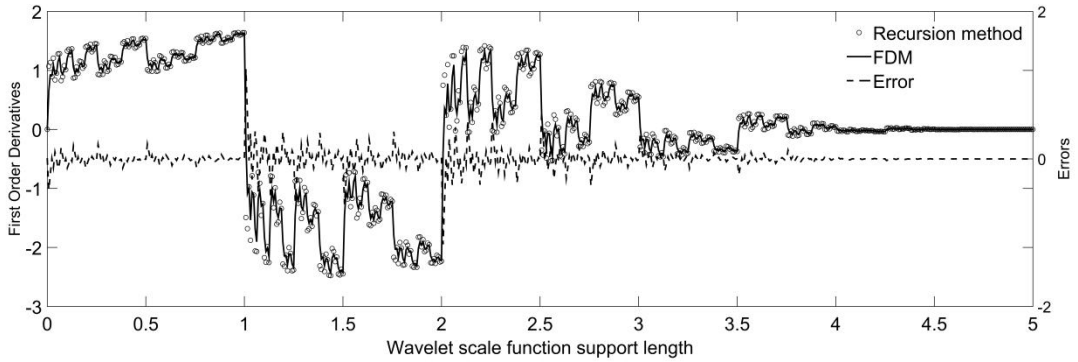


Fig. 2 First order derivatives of D6 scale function calculated by recursion method and FDM, with relative errors between them.

Integration needs to be carried out to obtained the mass and stiffness matrices expressed by Eq. and Eq.. To that end, the previously obtained two-scale relationship in terms of derivative calculation can be used in Eq.(13). By following the same

procedure, recursive relationship could also be established for integration calculation [15, 16]. Or alternatively, numerical scheme could be used to directly calculate the integration terms [17].

## 3 Results and discussions

The application of the WDRM in the analysis of high-frequency vibrations is demonstrated in this section using a uniform Euler-Bernoulli beam. This is a good benchmark problem which allows exact solutions. Results on both free and forced vibration problems are presented in the following two subsections. It should be mentioned that the validity of the Euler-Bernoulli assumption at high-frequency range is well known and is beyond the main scope of the present paper, since the main purpose is for illustrating the efficiency and the accuracy of the method through comparison with a simple benchmark problem with exact solutions.

### 3.1 Eigen-frequency study

The eigen-frequency problem described by Eq. is first considered in this subsection. Both free-free and pinned-pinned boundary conditions are considered. The eigen-frequencies are respectively given bellow [18]

$$f_{n_1} = \frac{(n+1/2)^2 p}{2l^2}\sqrt{\frac{EI}{rA}}, \quad \text{for } n > 5, \text{ free-free} \tag{25}$$

$$f_{n_2} = \frac{n^2 p}{2l^2}\sqrt{\frac{EI}{rA}} \quad \text{pined-pined} \tag{26}$$

where $A$ is the cross section area of the beam. In the calculations, parameters of the beam are chosen as $r = 7800\mathrm{kg/m^3}$, $l = 0.1\mathrm{m}$, $B = 0.01\mathrm{m}$, $h = 0.025\mathrm{m}$, $E = 2.1\mathrm{E}11\mathrm{Pa}$. Various stiffness terms are set as: $k_1 = k_2 = 0$, $q_1 = q_2 = 0$ for free-free boundary conditions; and $k_1 = k_2 = 5\mathrm{E}16\ \mathrm{N/m}$, $q_1 = q_2 = 0$ for pinned-pinned boundaries. Compared with the nominal stiffness of the beam ($k_0=EI/l^3$), these values correspond to a non-dimensional parameter $k_i/k_0$ = 1.83E13 for both $k_1$ and $k_2$. The convergence has been carefully checked to show that further increases in $k_i$ would not lead to noticeable changes in the calculated results.

The accuracy of the WDRM is tested through error analyses and convergence study respectively. This leads to the final selection of the parameters used in the calculation: $L$=16 and $m$=8, resulting in 2574 wavelet scale function items. The calculated natural frequencies are tabulated in Table 1, in comparison with analytical ones. Note all first 1100 modes were successfully obtained. For the sake of briefness, only three representative groups, corresponding to low, middle and high-frequency bands, are tabulated in Table 1. The first column in each sub-table is the mode number, including free-free (F-F) and pinned-pinned (P-P) boundary conditions of the beam. '*(A)*' and '*(W)*' are abbreviation for analytical method and WDRM, respectively. It is noted that the WDRM achieves remarkable accuracy as compared with the analytical results in both boundary cases in all three frequency bands.

In order to quantify the accuracy of the proposed WDRM, the relative error for each eigen-frequency is defined as

$$h = \frac{\left| f_{exact} - f_{w} \right|}{f_{exact}} \cdot 100\% \tag{27}$$

where $f_{exact}$ is the exact frequency value and $f_{w}$ the numerically calculated eigen-frequency by WDRM. The relative error for all 1100 calculated natural frequencies is shown in Fig.3. Generally speaking, the relative error for both boundary conditions is very small for basically the first half of modes. Errors start to increase for higher-order modes. Nevertheless, the agreement between the WDRM results and analytical ones is caped under 1% for all modes, which is excellent considering the fact that it is a 1-D configuration. For a 2-D case, with all cross terms among the two directions, the number of modes that could be correctly predicted should be phenomenal.

Typical mode shapes are also checked against the analytical ones. Shown in Fig. 4, three modes (1st, 500th and 1000th) are illustrated, showing perfect agreement with analytical results. In order to have a clear view of the mode shape, only part of the beam is used in the illustrations for mode 500 (0-2cm) and mode 1000 (0-1cm) due to their very small wavelengths.

## Table 1

*Comparison of the eigen-frequencies in low frequency, middle and high frequency bands*

| Low Frequency Band | | | | |
|---|---|---|---|---|
| No. | F-F (A) | F-F (W) | P-P (A) | S-S (W) |
| 5 | 0.1779E5 | 0.1779E5 | 0.1471E5 | 0.1471E5 |
| 6 | 0.2485E5 | 0.2485E5 | 0.2118E5 | 0.2118E5 |
| 7 | 0.3309E5 | 0.3309E5 | 0.2882E5 | 0.2882E5 |
| 8 | 0.4250E5 | 0.4250E5 | 0.3765E5 | 0.3765E5 |
| 9 | 0.5309E5 | 0.5309E5 | 0.4764E5 | 0.4764E5 |
| 10 | 0.6485E5 | 0.6485E5 | 0.5882E5 | 0.5882E5 |
| 11 | 0.7779E5 | 0.7779E5 | 0.7117E5 | 0.7117E5 |
| 12 | 0.9191E5 | 0.9191E5 | 0.8470E5 | 0.8470E5 |
| 13 | 1.0720E5 | 1.0720E5 | 0.9941E5 | 0.9941E5 |
| 14 | 1.2367E5 | 1.2367E5 | 1.1529E5 | 1.1529E5 |
| 15 | 1.4132E5 | 1.4132E5 | 1.3235E5 | 1.3235E5 |
| 16 | 1.6014E5 | 1.6014E5 | 1.5058E5 | 1.5058E5 |
| 17 | 1.8014E5 | 1.8014E5 | 1.6999E5 | 1.6999E5 |
| 18 | 2.0131E5 | 2.0131E5 | 1.9058E5 | 1.9058E5 |
| 19 | 2.2367E5 | 2.2367E5 | 2.1234E5 | 2.1234E5 |
| 20 | 2.4719E5 | 2.4719E5 | 2.3528E5 | 2.3528E5 |
| 21 | 2.7190E5 | 2.7190E5 | 2.5940E5 | 2.5940E5 |
| 22 | 2.9778E5 | 2.9778E5 | 2.8469E5 | 2.8469E5 |
| 23 | 3.2484E5 | 3.2484E5 | 3.1116E5 | 3.1116E5 |
| 24 | 3.5307E5 | 3.5307E5 | 3.3881E5 | 3.3881E5 |
| 25 | 3.8248E5 | 3.8248E5 | 3.6763E5 | 3.6763E5 |
| 26 | 4.1307E5 | 4.1307E5 | 3.9763E5 | 3.9763E5 |
| 27 | 4.4483E5 | 4.4483E5 | 4.2880E5 | 4.2880E5 |
| 28 | 4.7777E5 | 4.7777E5 | 4.6116E5 | 4.6116E5 |
| 29 | 5.1189E5 | 5.1189E5 | 4.9468E5 | 4.9468E5 |
| 30 | 5.4718E5 | 5.4718E5 | 5.2939E5 | 5.2939E5 |
| 31 | 5.8365E5 | 5.8365E5 | 5.6527E5 | 5.6527E5 |
| 32 | 6.2130E5 | 6.2130E5 | 6.0233E5 | 6.0233E5 |
| 33 | 6.6012E5 | 6.6012E5 | 6.4056E5 | 6.4056E5 |
| 34 | 7.0012E5 | 7.0012E5 | 6.7997E5 | 6.7997E5 |

| Middle Frequency Band | | | | |
|---|---|---|---|---|
| No. | F-F | F-F (W) | P-P (A) | P-P (W) |
| 505 | 1.5031 | 1.5030E8 | 1.5001E8 | 1.5000E8 |
| 506 | 1.5090 | 1.5090E8 | 1.5060E8 | 1.5060E8 |
| 507 | 1.5150 | 1.5150E8 | 1.5120E8 | 1.5119E8 |
| 508 | 1.5209 | 1.5209E8 | 1.5180E8 | 1.5179E8 |
| 509 | 1.5269 | 1.5269E8 | 1.5239E8 | 1.5239E8 |
| 510 | 1.5329 | 1.5329E8 | 1.5299E8 | 1.5299E8 |
| 511 | 1.5389 | 1.5389E8 | 1.5359E8 | 1.5359E8 |
| 512 | 1.5450 | 1.5450E8 | 1.5420E8 | 1.5419E8 |
| 513 | 1.5510 | 1.5510E8 | 1.5480E8 | 1.5479E8 |
| 514 | 1.5570 | 1.5570E8 | 1.5540E8 | 1.5540E8 |
| 515 | 1.5631 | 1.5631E8 | 1.5601E8 | 1.5600E8 |
| 516 | 1.5692 | 1.5692E8 | 1.5661E8 | 1.5661E8 |
| 517 | 1.5753 | 1.5753E8 | 1.5722E8 | 1.5722E8 |
| 518 | 1.5814 | 1.5813E8 | 1.5783E8 | 1.5783E8 |
| 519 | 1.5875 | 1.5875E8 | 1.5844E8 | 1.5844E8 |
| 520 | 1.5936 | 1.5936E8 | 1.5905E8 | 1.5905E8 |
| 521 | 1.5997 | 1.5997E8 | 1.5966E8 | 1.5966E8 |
| 522 | 1.6058 | 1.6058E8 | 1.6028E8 | 1.6027E8 |
| 523 | 1.6120 | 1.6120E8 | 1.6089E8 | 1.6089E8 |
| 524 | 1.6182 | 1.6182E8 | 1.6151E8 | 1.6150E8 |
| 525 | 1.6243 | 1.6243E8 | 1.6213E8 | 1.6212E8 |
| 526 | 1.6305 | 1.6305E8 | 1.6274E8 | 1.6274E8 |
| 527 | 1.6367 | 1.6367E8 | 1.6336E8 | 1.6336E8 |
| 528 | 1.6429 | 1.6429E8 | 1.6398E8 | 1.6398E8 |
| 529 | 1.6492 | 1.6492E8 | 1.6460E8 | 1.6460E8 |
| 530 | 1.6554 | 1.6554E8 | 1.6523E8 | 1.6522E8 |
| 531 | 1.6616 | 1.6616E8 | 1.6585E8 | 1.6585E8 |
| 532 | 1.6679 | 1.6679E8 | 1.6648E8 | 1.6647E8 |
| 533 | 1.6742 | 1.6742E8 | 1.6710E8 | 1.6710 E8 |
| 534 | 1.6805 | 1.6804E8 | 1.6773E8 | 1.6773 E8 |

| High Frequency Band | | | | |
|---|---|---|---|---|
| No. | F-F (A) | F-F (W) | P-P (A) | P-P (W) |
| 1005 | 5.9470E8 | 5.9469E8 | 5.9411E8 | 5.9409 E8 |
| 1006 | 5.9588E8 | 5.9588E8 | 5.9529E8 | 5.9527 E8 |
| 1007 | 5.9707E8 | 5.9706E8 | 5.9647E8 | 5.9646 E8 |
| 1008 | 5.9825E8 | 5.9825E8 | 5.9766E8 | 5.9764 E8 |
| 1009 | 5.9944E8 | 5.9944E8 | 5.9884E8 | 5.9883 E8 |
| 1010 | 6.0063E8 | 6.0062E8 | 6.0003E8 | 6.0002 E8 |
| 1011 | 6.0182E8 | 6.0181E8 | 6.0122E8 | 6.0121 E8 |
| 1012 | 6.0301E8 | 6.0300E8 | 6.0241E8 | 6.0240 E8 |
| 1013 | 6.0420E8 | 6.0420E8 | 6.0360E8 | 6.0359 E8 |
| 1014 | 6.0539E8 | 6.0539E8 | 6.0479E8 | 6.0478 E8 |
| 1015 | 6.0658E8 | 6.0658E8 | 6.0599E8 | 6.0597 E8 |
| 1016 | 6.0778E8 | 6.0778E8 | 6.0718E8 | 6.0717 E8 |
| 1017 | 6.0898E8 | 6.0897E8 | 6.0838E8 | 6.0836 E8 |
| 1018 | 6.1017E8 | 6.1017E8 | 6.0958E8 | 6.0956 E8 |
| 1019 | 6.1137E8 | 6.1137E8 | 6.1077E8 | 6.1076 E8 |
| 1020 | 6.1257E8 | 6.1257E8 | 6.1197E8 | 6.1196 E8 |
| 1021 | 6.1377E8 | 6.1377E8 | 6.1317E8 | 6.1316 E8 |
| 1022 | 6.1498E8 | 6.1497E8 | 6.1437E8 | 6.1436 E8 |
| 1023 | 6.1618E8 | 6.1618E8 | 6.1558E8 | 6.1556 E8 |
| 1024 | 6.1738E8 | 6.1738E8 | 6.1678E8 | 6.1677 E8 |
| 1025 | 6.1859E8 | 6.1859E8 | 6.1799E8 | 6.1797 E8 |
| 1026 | 6.1980E8 | 6.1979E8 | 6.1919E8 | 6.1918 E8 |
| 1027 | 6.2101E8 | 6.2100E8 | 6.2040E8 | 6.2038 E8 |
| 1028 | 6.2221E8 | 6.2221E8 | 6.2161E8 | 6.2159 E8 |
| 1029 | 6.2343E8 | 6.2342E8 | 6.2282E8 | 6.2280 E8 |
| 1030 | 6.2464E8 | 6.2463E8 | 6.2403E8 | 6.2401 E8 |
| 1031 | 6.2585E8 | 6.2585E8 | 6.2524E8 | 6.2523 E8 |
| 1032 | 6.2706E8 | 6.2706E8 | 6.2646E8 | 6.2644 E8 |
| 1033 | 6.2828E8 | 6.2828E8 | 6.2767E8 | 6.2766 E8 |
| 1034 | 6.2950E8 | 6.2949E8 | 6.2889E8 | 6.2887 E8 |

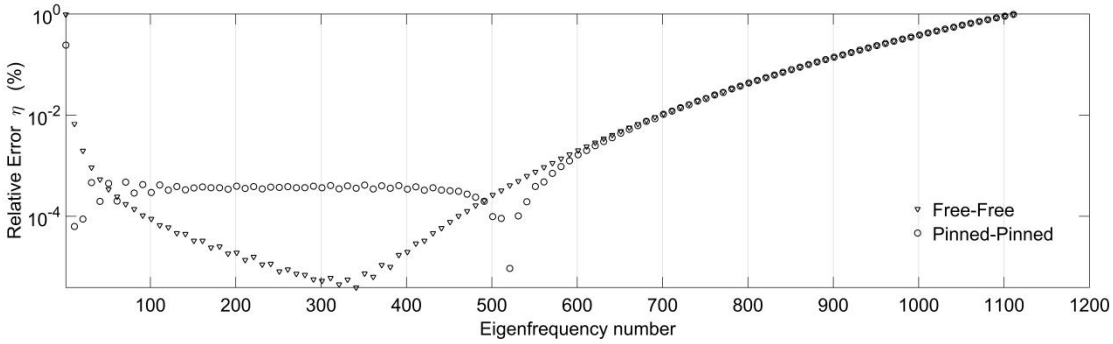


Fig. 3 Relative error compared with exact solution, using wavelet resolution m=8, support length L=16, considering both the free-free and pinned-pinned boundary conditions.

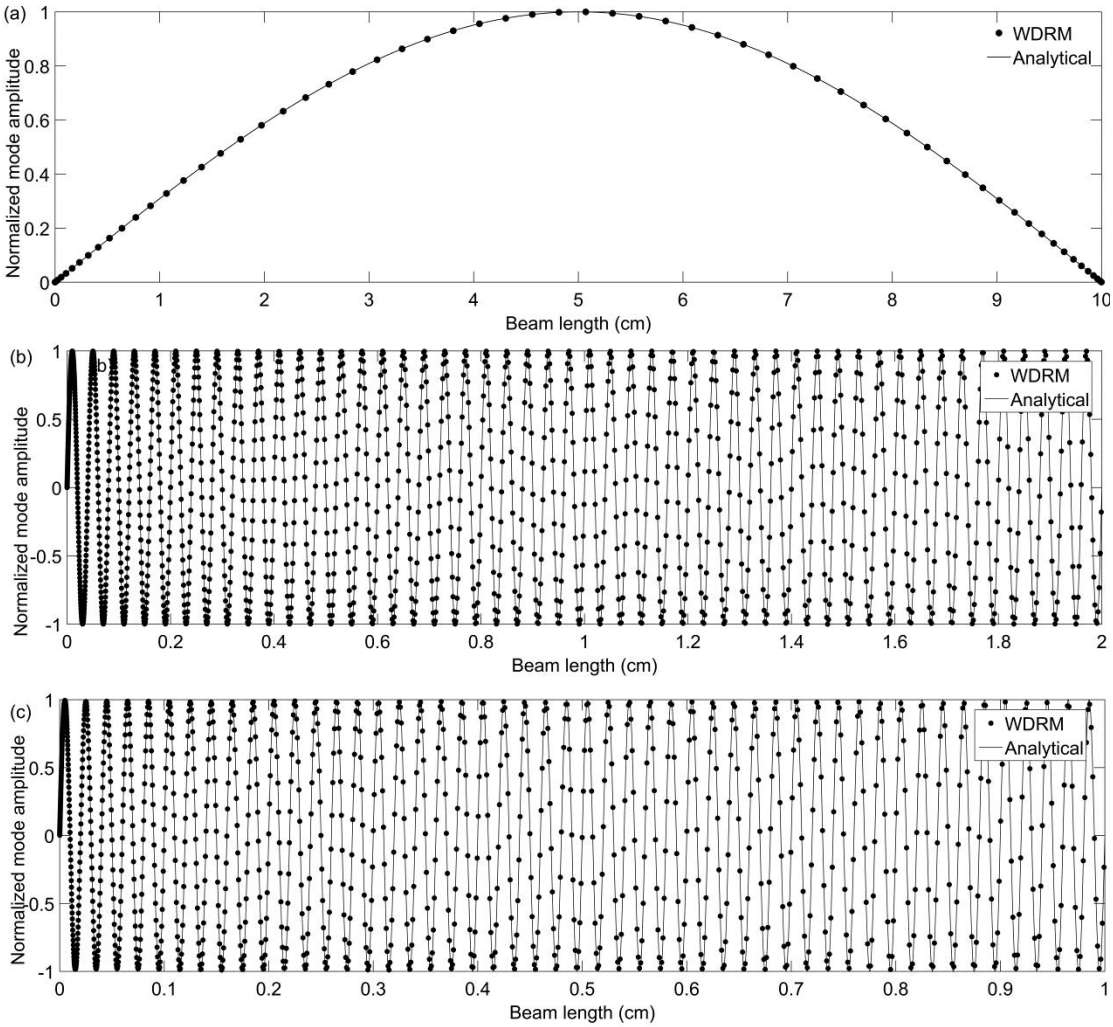


Fig. 4 Mode shape comparison between WDRM and analytical method: (a) 1st mode within beam length 0-10cm (b) 500th mode within beam length 0-2cm. (c) 1000th mode with beam length 0-1cm.

To examine the convergence of the proposed WDRM, the relative error is examined with varying resolution parameter *m*, as shown in Fig. 5. As can be seen, *m* needs to be increased for the same support length L for more modes to be correctly calculated. More specifically, when *m*=4, about 70 eigen-frequencies can be obtained under 1% error. The number increases to about 280 for *m*=6; and 1100 for m=8. Therefore, the effect of the resolution parameter is obvious. When fixing *m*, however, results show little influence of the support length, L, (not shown here).

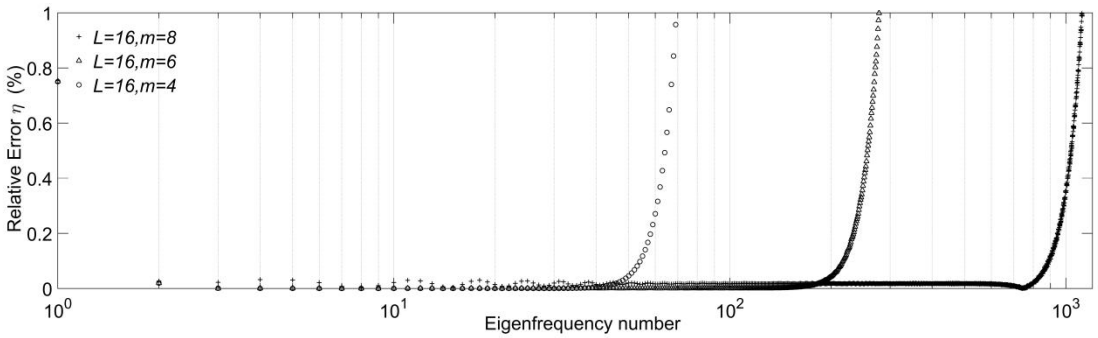


Fig. 5 Relative error within 1% threshold for different Daubechies wavelet scale function resolution *m* while the support length *L* is fixed at 16.

### 3.2 Forced vibration response

Forced vibration response of the beam is calculated to further verify the accuracy of the proposed method. A unit excitation force is located at $x_F$=2cm as shown in Fig.1. The response of the pined-pined beam, at an arbitrarily chosen location *x*=9cm, is given in Fig. 6, covering a wide frequency band between 100Hz to 100kHz. The analytical solution, used as reference for comparison, writes [18]

$$w(x) = \frac{2}{rA1}\sum_{n=1}^{\infty}\frac{1}{w_n^2 - w^2}\sin\left(\frac{n\pi x_F}{1}\right)\sin\left(\frac{n\pi x}{1}\right) \tag{28}$$

To generate accurate analytical results, ten thousand modes were used in the calculation using Eq.(28). In all three frequency bands, low in Figs. 6(a), middle in Figs. 6(b) and high in Figs. 6(c), the displacement responses calculated by the WDRM are almost identical to the analytical solutions, demonstrating again the remarkable accuracy of the method, even for very high frequencies.

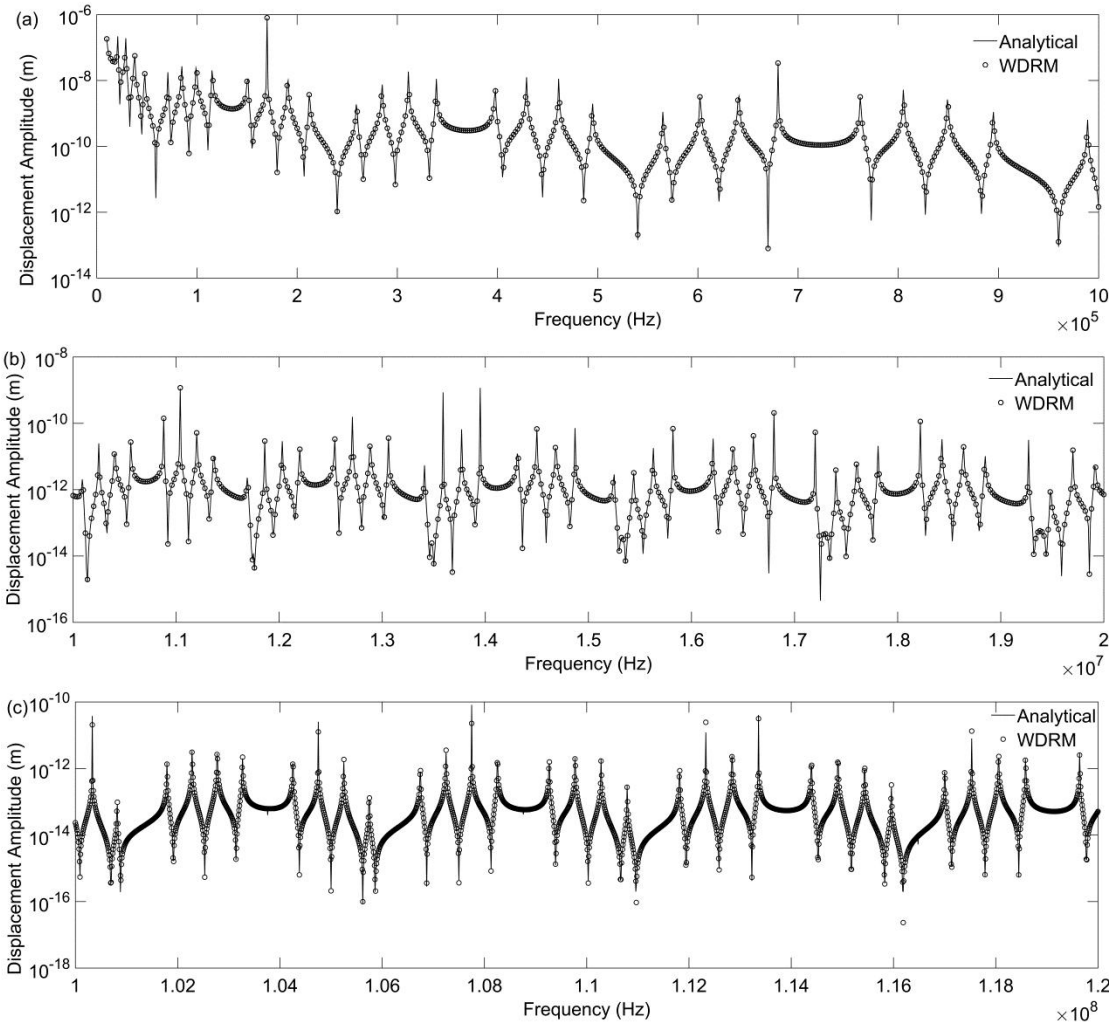


Fig. 6. Displacement amplitude at specific locations in different frequency bands: (a) $x$=9cm with the frequency band from 100Hz to 10kHz, (b) $x$=9cm with the frequency

band from 10Mhz to 20Mhz, (c) $x$=9cm with the frequency band from 0.1GHz to 0.12GHz.

Furthermore, Fig. 7 shows the displacement amplitude along the beam at three representative frequencies, taken from Fig.6. As can be seen, for all three frequencies, WDRM and analytical method provide almost the same results. Note again that, due to the extremely tightness of the wave at high frequency, only one-tenth of the beam length is shown in Fig. 7(c).

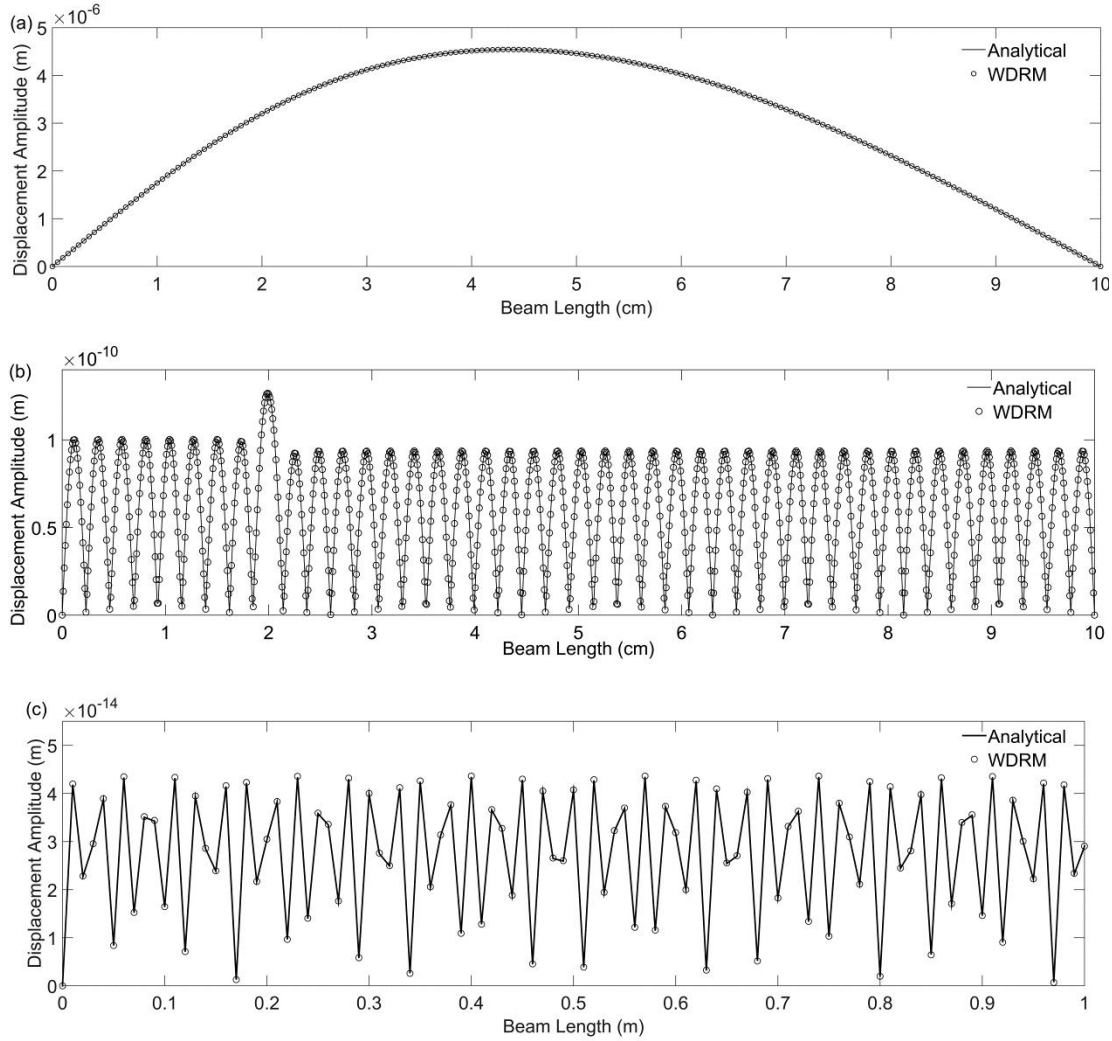


Fig.7 Displacement amplitude along the beam at specific frequencies: (a) 100Hz from 0cm to 10cm. b)1.1MHz from 0 cm to 10cm. (c) 0.1GHz from 0cm to1cm (only part

of the beam).

It is relevant to comment on a few important issues related to Daubechies wavelet scale functions and their use as decomposition basis under the current Rayleigh-Ritz framework. First, Daubechies wavelet scale functions are known to possess unique features such as compact support, flexible scaling and translation, and the ability to express any square integrable function on the real axis. This leads to their extraordinary fitting ability in approximating both highly oscillating and smooth functions, as demonstrated earlier in acoustic predictions [12], and again confirmed here in the present vibration study. This guarantees much better convergence as opposed to the trigonometric functions. Meanwhile, it could also minimize the round-off errors which could lead to ill-conditioned matrices like in the case of polynomials. Second, the calculation efficiency of the propose WDRM is worth noting. Owing to the compact support property of the Daubechies wavelet scale functions, the resulting mass and stiffness matrices are band limited, with all non-zero terms concentrated along the diagonal band. The bandwidth is $L$-1, where $L$ is the support length of the Daubechies wavelet scale functions. Thanks to this bandlimited property, the solving process is straightforward and very efficient. As an indicative example of the present 1-D problem, using $L$=16, $m$=6 leads to 654 by 654 matrices, the calculation of the natural modes roughly takes about 1 minute on a conventional 64-bits Dell workstation with a 3GHz CPU to get the first 280th mode within 1% error. Limited by the maximum ram of the workstation (64GB), the true limit of the method was not reached in our investigation. Lastly, it is relevant to mention that, the established approach exhibits its flexibility in dealing with various structural boundaries. In that sense, the Daubechies wavelet scale functions can be generally applied since the parameters involved are independent of the physical boundary

conditions of the structure.

As a general remark, it is relevant to note that an Euler-Bernoulli beam is used as a representative dynamic system to illustrate the issue. There should be no particular technical obstacles to apply the proposed Wavelet-decomposed approach to more complex systems, which would also benefit from the efficacy of the approach, similar to what has been demonstrated in this paper.

## 4 Conclusions

This paper explores the use of wavelet decomposition under the general framework of Rayleigh-Ritz method for high-frequency vibration analyses. Using a benchmark problem of Euler-Bernoulli beam, the efficacy of the proposed wavelet-decomposed Rayleigh-Ritz method is demonstrated. Wavelet basis provides localized compact support, which leads to sparse representations of the system matrices. Along with its exceptional fitting ability and the treatment of the structural boundary using artificial springs, the proposed approach exhibits tremendous computational advantages and allows reaching extremely high frequency range. The proposed approach combines the flexibility of the global methods and the accuracy of local methods by inheriting the versatility of the Rayleigh-Ritz approach and the unique feature of the wavelets. More specifically, more than one thousand modes are correctly predicted in the present configuration with an error of less than 1% using conventional computational

facility. Forced vibration responses also show excellent agreement with analytical solutions within the range covered by the same group of modes. To our knowledge, the frequency coverage and the level of accuracy achieved outperform what can be found in the open literature using Rayleigh-Ritz methods. It can be anticipated that, upon extension to 2D cases, the number of modes that could be accurately predicted should be at least a few order of magnitude higher, which potentially might accommodate the need for structural analyses and design in a very broad frequency range.

**Acknowledgements**

The authors wish to acknowledge a grant from Research Grants Council of Hong Kong Special Administrative Region, China (PolyU 152026/14E)

## References


1. R. S. Langley, N. S. Bardell, A review of current analysis capabilities applicable to the high frequency vibration prediction of aerospace structures , *Aeronautical Journal* 102 (1998) 287-297.
2. L. Cheng, J. Nicolas, Free vibration analysis of a cylindrical shell – circular plate system with general coupling and various boundary conditions, *Journal of Sound and Vibration* 155 (1992) 231–247.
3. L. Cheng, R. Lapointe, Vibration attenuation of panel structures by optimally shaped viscoelastic coating with added weight considerations, *Thin-walled structures* 21 (1995) 307-326.
4. A. Berry, J. L. Guyader, J. Nicolas, A general formulation for the sound radiation from rectangular, baffled plates with arbitrary boundary conditions, *Journal of the Acoustical Society of America* 88 (1990) 2792-2802.
5. J. P. Webb, R. Abouchacra, Hierarchal triangular elements using orthogonal polynomials, *International Journal for Numerical Methods in Engineering* 38 (1995) 245–257.
6. N. S. Bardell, Free vibration analysis of a flat plate using the hierarchical finite element method , *Journal of sound and vibration* 151 (1991) 263-289.
7. P. Ruta, Application of Chebyshev series to solution of non-prismatic beam vibration problem, *Journal of Sound and vibration* 227 (1999) 449-467.
8. O. Beslin, J. Nicolas, A hierarchical functions set for predicting very high order plate bending modes with any boundary conditions, *Journal of Sound and Vibration* 202 (1997) 633-655.
9. D. Zhou, Natural frequencies of rectangular plates using a set of static beam functions in Rayleigh-Ritz method, *Journal of Sound and Vibration* 189 **(**1996**)** 81-87.
10. W. L. Li, Free vibrations of beams with general boundary conditions, *Journal of Sound and Vibration* 237 (2000) 709-725.
11. W. L. Li, M. Daniels, A Fourier series method for the vibrations of elastically restrained plates arbitrarily loaded with springs and masses, *Journal of Sound and Vibration* 252 (2002) 768-781.
12. S. Zhang, L. Cheng, Shape optimization of acoustic enclosures based on a wavelet–Galerkin formulation, *International Journal of Applied Mechanics* 7 (2015) 1550009.
13. A. Cohen, Numerical analysis of wavelet methods, Elsevier, Amsterdam, 2003.
14. M. Q. Chen, C. Hwang, Y. P. Shih, The computation of wavelet−Galerkin approximation on a bounded interval, *International Journal for Numerical Methods in Engineering* 39 (1996) 2921-2944.
15. G. Beylkin, On the representation of operators in bases of compactly supported wavelets,

*SIAM Journal on Numerical Analysis* 29 (1992) 1716-1740.

16. W. Dahmen, L. Micchel, A. Charles, Using the refinement equation for evaluating integrals of wavelets, *SIAM Journal on Numerical Analysis*, 30 (1993) 507-537.
17. K. Maleknejad, M. Yousefi, K. Nouri, Computational methods for integrals involving functions and Daubechies wavelets , *Applied Mathematics and Computation* 189 (2007) 1828–1840.
18. S. S. Rao, F. F. Yap, Mechanical vibrations, Prentice Hall, London, 2011.

**Figures and Tables Caption**

Fig.1 Euler-Bernoulli beam model.

Fig. 2 First order derivatives of D6 scale function calculated by recursion method and FDM, with relative errors between them.

Fig. 3 Relative error compared with exact solution, using wavelet resolution m=8, support length L=16, considering both the free-free and pinned-pinned boundary conditions.

Fig. 4 Mode shape comparison between WDRM and analytical method: (a) 1st mode within beam length 0-10cm (b) 500th mode within beam length 0-2cm. (c) 1000th mode with beam length 0-1cm.

Fig. 5 Relative error within 1% threshold for different Daubechies wavelet scale function resolution m while the support length L is fixed at 16.

Fig. 6. Displacement amplitude at specific locations in different frequency bands: (a) x=9cm with the frequency band from 100Hz to 10kHz, (b) x=9cm with the frequency band from 10Mhz to 20Mhz, (c) x=9cm with the frequency band from 0.1GHz to 0.12GHz.

Fig.7 Displacement amplitude along the beam at specific frequencies: (a) 100Hz from 0cm to 10cm. b)1.1MHz from 0 cm to 10cm. (c) 0.1GHz from 0cm to1cm (only part of the beam).

Table 1 Comparison of the eigen-frequencies in low frequency, middle and high frequency bands

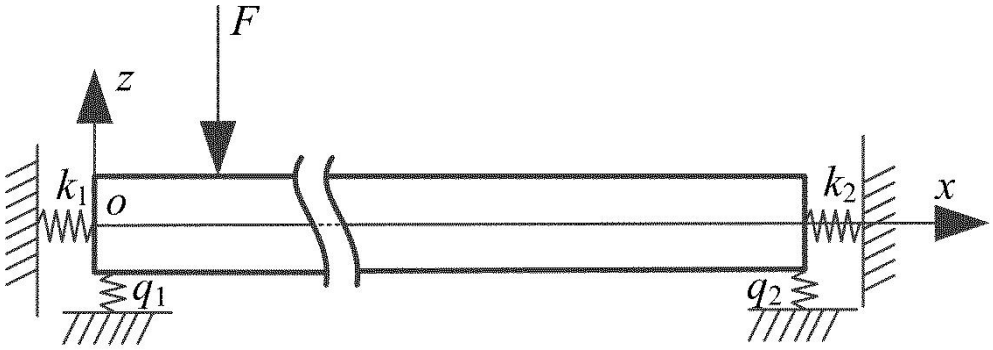


Fig.1 Euler-Bernoulli beam model.

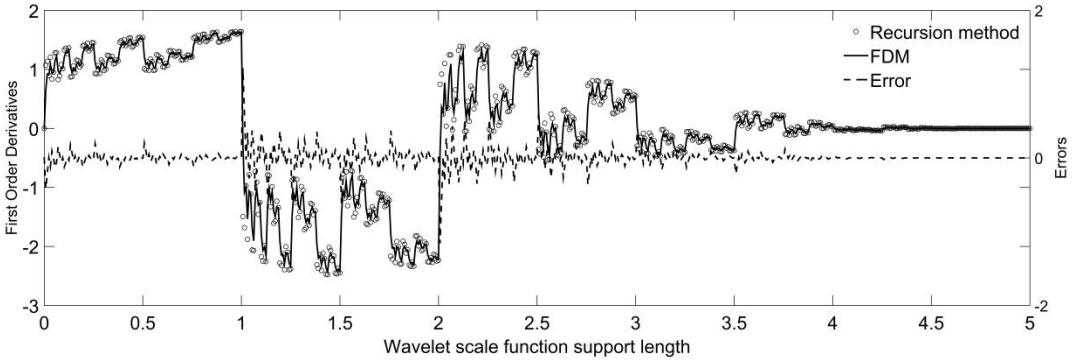


Fig. 2 First order derivatives of D6 scale function calculated by recursion method and FDM, with relative errors between them.

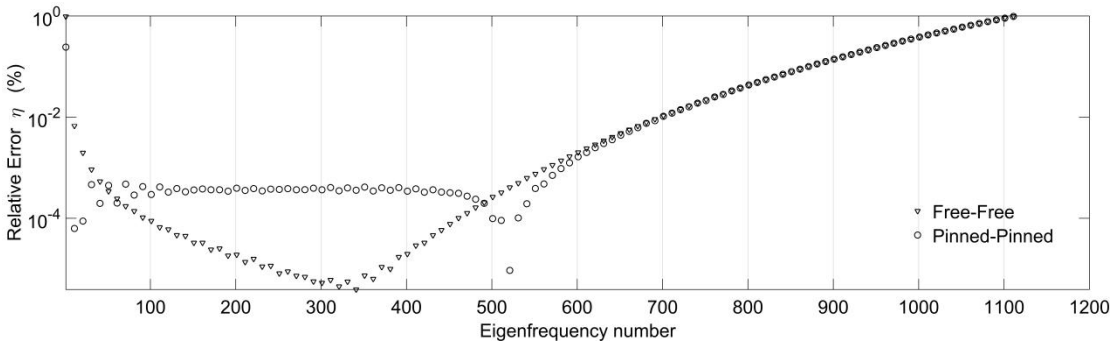


Fig. 3 Relative error compared with exact solution, using wavelet resolution m=8, support length L=16, considering both the free-free and pinned-pinned boundary conditions.

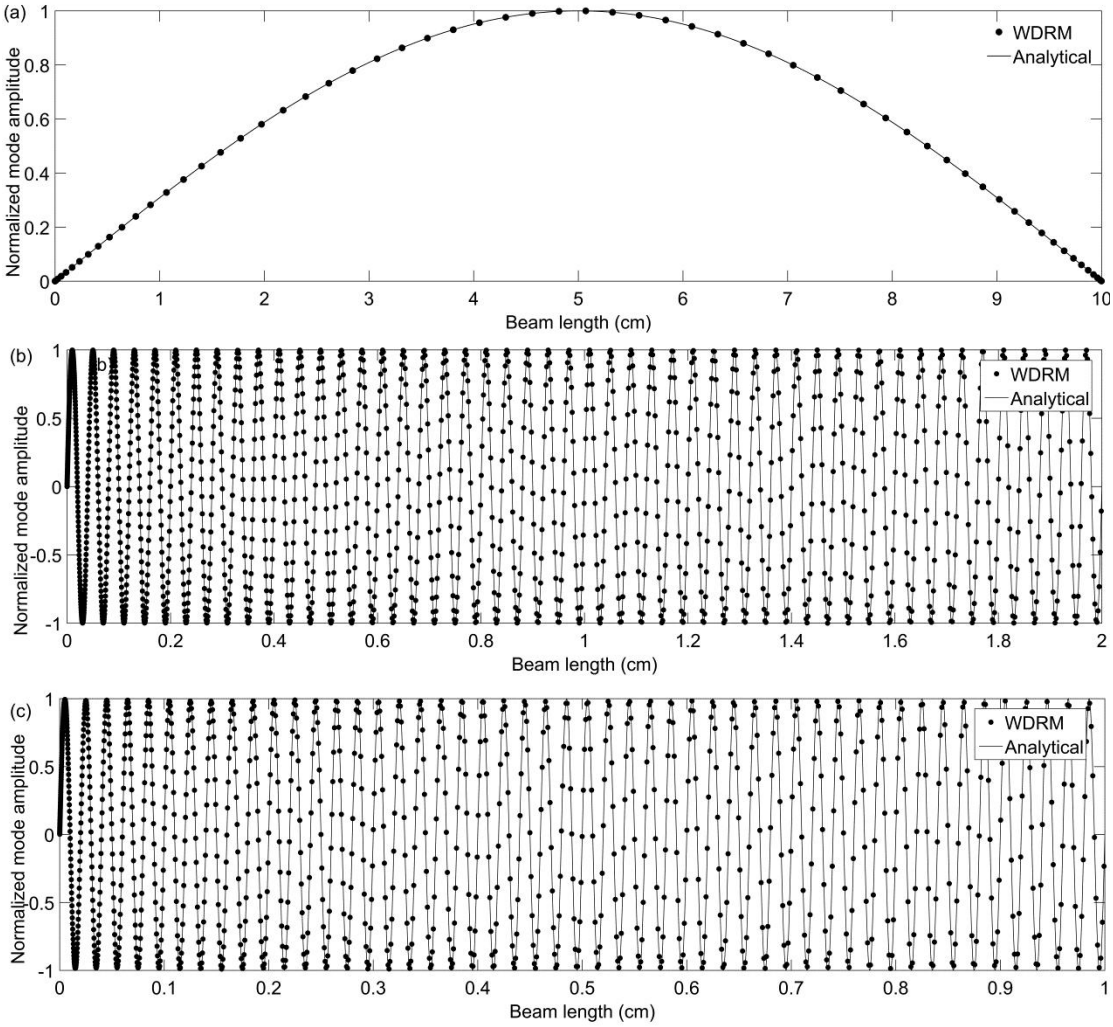


Fig. 4 Mode shape comparison between WDRM and analytical method: (a) 1st mode within beam length 0-10cm (b) 500th mode within beam length 0-2cm. (c) 1000th mode with beam length 0-1cm.

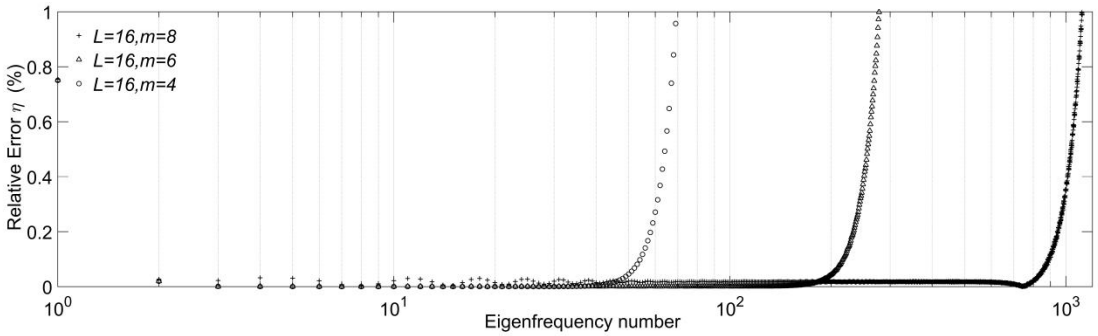


Fig. 5 Relative error within 1% threshold for different Daubechies wavelet scale function resolution *m* while the support length *L* is fixed at 16.

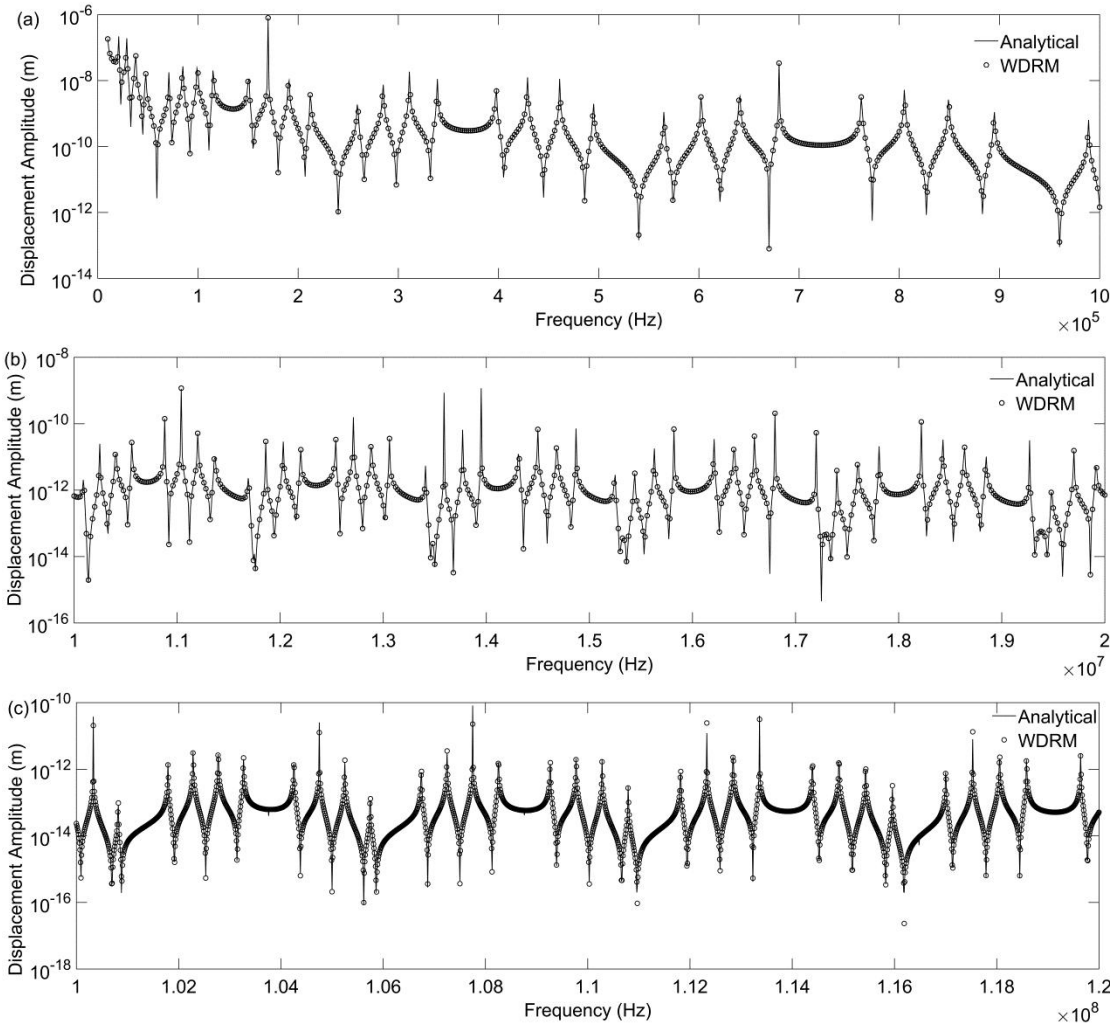


Fig. 6. Displacement amplitude at specific locations in different frequency bands: (a) $x$=9cm with the frequency band from 100Hz to 10kHz, (b) $x$=9cm with the frequency band from 10Mhz to 20Mhz, (c) $x$=9cm with the frequency band from 0.1GHz to 0.12GHz.

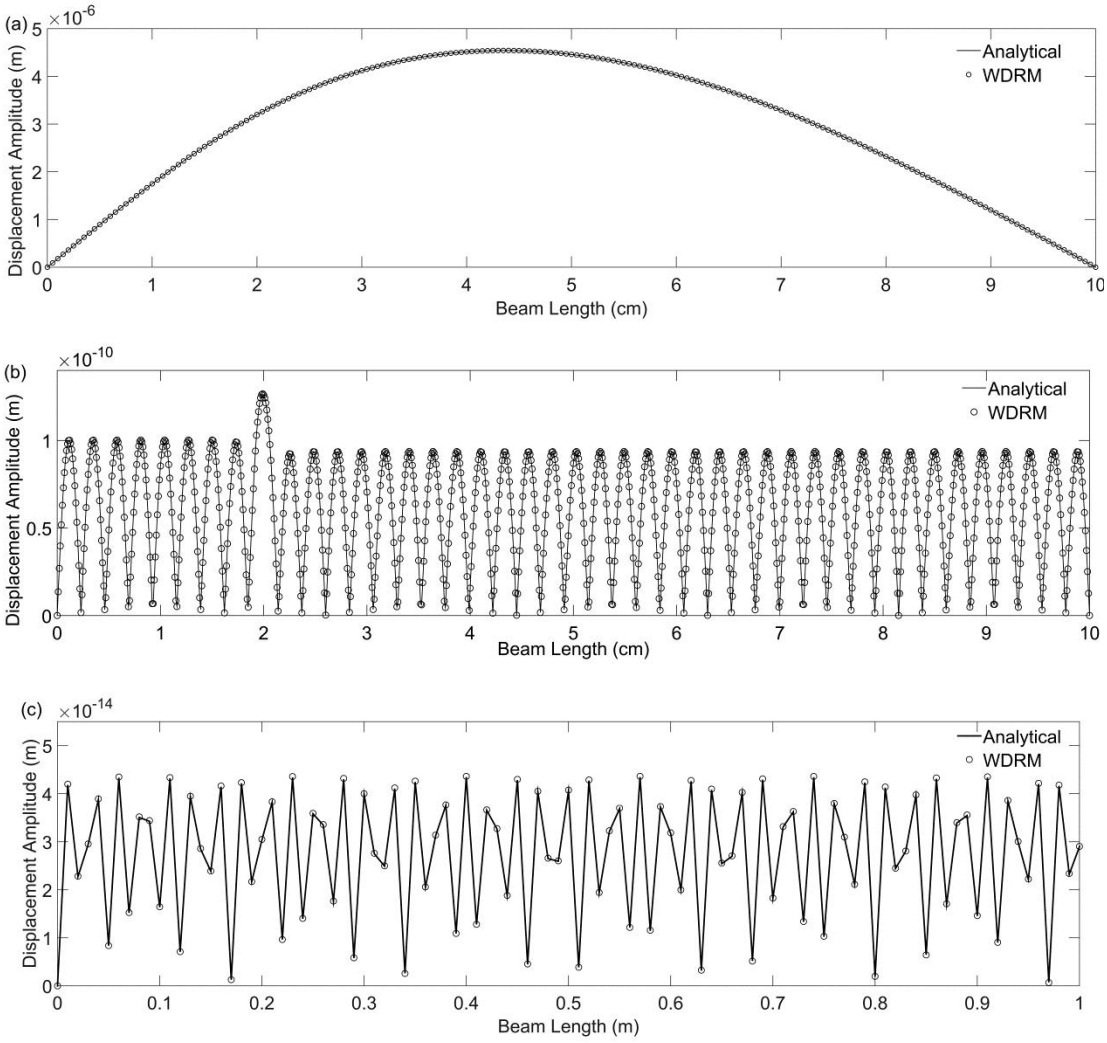


Fig.7 Displacement amplitude along the beam at specific frequencies: (a) 100Hz from 0cm to 10cm. b)1.1MHz from 0 cm to 10cm. (c) 0.1GHz from 0cm to1cm (only part of the beam).

## Table 1

*Comparison of the eigen-frequencies in low frequency, middle and high frequency bands*

| Low Frequency Band | | | | |
|---|---|---|---|---|
| No. | F-F (A) | F-F (W) | P-P (A) | S-S (W) |
| 5 | 0.1779E5 | 0.1779E5 | 0.1471E5 | 0.1471E5 |
| 6 | 0.2485E5 | 0.2485E5 | 0.2118E5 | 0.2118E5 |
| 7 | 0.3309E5 | 0.3309E5 | 0.2882E5 | 0.2882E5 |
| 8 | 0.4250E5 | 0.4250E5 | 0.3765E5 | 0.3765E5 |
| 9 | 0.5309E5 | 0.5309E5 | 0.4764E5 | 0.4764E5 |
| 10 | 0.6485E5 | 0.6485E5 | 0.5882E5 | 0.5882E5 |
| 11 | 0.7779E5 | 0.7779E5 | 0.7117E5 | 0.7117E5 |
| 12 | 0.9191E5 | 0.9191E5 | 0.8470E5 | 0.8470E5 |
| 13 | 1.0720E5 | 1.0720E5 | 0.9941E5 | 0.9941E5 |
| 14 | 1.2367E5 | 1.2367E5 | 1.1529E5 | 1.1529E5 |
| 15 | 1.4132E5 | 1.4132E5 | 1.3235E5 | 1.3235E5 |
| 16 | 1.6014E5 | 1.6014E5 | 1.5058E5 | 1.5058E5 |
| 17 | 1.8014E5 | 1.8014E5 | 1.6999E5 | 1.6999E5 |
| 18 | 2.0131E5 | 2.0131E5 | 1.9058E5 | 1.9058E5 |
| 19 | 2.2367E5 | 2.2367E5 | 2.1234E5 | 2.1234E5 |
| 20 | 2.4719E5 | 2.4719E5 | 2.3528E5 | 2.3528E5 |
| 21 | 2.7190E5 | 2.7190E5 | 2.5940E5 | 2.5940E5 |
| 22 | 2.9778E5 | 2.9778E5 | 2.8469E5 | 2.8469E5 |
| 23 | 3.2484E5 | 3.2484E5 | 3.1116E5 | 3.1116E5 |
| 24 | 3.5307E5 | 3.5307E5 | 3.3881E5 | 3.3881E5 |
| 25 | 3.8248E5 | 3.8248E5 | 3.6763E5 | 3.6763E5 |
| 26 | 4.1307E5 | 4.1307E5 | 3.9763E5 | 3.9763E5 |
| 27 | 4.4483E5 | 4.4483E5 | 4.2880E5 | 4.2880E5 |
| 28 | 4.7777E5 | 4.7777E5 | 4.6116E5 | 4.6116E5 |
| 29 | 5.1189E5 | 5.1189E5 | 4.9468E5 | 4.9468E5 |
| 30 | 5.4718E5 | 5.4718E5 | 5.2939E5 | 5.2939E5 |
| 31 | 5.8365E5 | 5.8365E5 | 5.6527E5 | 5.6527E5 |
| 32 | 6.2130E5 | 6.2130E5 | 6.0233E5 | 6.0233E5 |
| 33 | 6.6012E5 | 6.6012E5 | 6.4056E5 | 6.4056E5 |
| 34 | 7.0012E5 | 7.0012E5 | 6.7997E5 | 6.7997E5 |

| Middle Frequency Band | | | | |
|---|---|---|---|---|
| No. | F-F (A) | F-F (W) | P-P (A) | P-P (W) |
| 505 | 1.5031E8 | 1.5030E8 | 1.5001E8 | 1.5000E8 |
| 506 | 1.5090E8 | 1.5090E8 | 1.5060E8 | 1.5060E8 |
| 507 | 1.5150E8 | 1.5150E8 | 1.5120E8 | 1.5119E8 |
| 508 | 1.5209E8 | 1.5209E8 | 1.5180E8 | 1.5179E8 |
| 509 | 1.5269E8 | 1.5269E8 | 1.5239E8 | 1.5239E8 |
| 510 | 1.5329E8 | 1.5329E8 | 1.5299E8 | 1.5299E8 |
| 511 | 1.5389E8 | 1.5389E8 | 1.5359E8 | 1.5359E8 |
| 512 | 1.5450E8 | 1.5450E8 | 1.5420E8 | 1.5419E8 |
| 513 | 1.5510E8 | 1.5510E8 | 1.5480E8 | 1.5479E8 |
| 514 | 1.5570E8 | 1.5570E8 | 1.5540E8 | 1.5540E8 |
| 515 | 1.5631E8 | 1.5631E8 | 1.5601E8 | 1.5600E8 |
| 516 | 1.5692E8 | 1.5692E8 | 1.5661E8 | 1.5661E8 |
| 517 | 1.5753E8 | 1.5753E8 | 1.5722E8 | 1.5722E8 |
| 518 | 1.5814E8 | 1.5813E8 | 1.5783E8 | 1.5783E8 |
| 519 | 1.5875E8 | 1.5875E8 | 1.5844E8 | 1.5844E8 |
| 520 | 1.5936E8 | 1.5936E8 | 1.5905E8 | 1.5905E8 |
| 521 | 1.5997E8 | 1.5997E8 | 1.5966E8 | 1.5966E8 |
| 522 | 1.6058E8 | 1.6058E8 | 1.6028E8 | 1.6027E8 |
| 523 | 1.6120E8 | 1.6120E8 | 1.6089E8 | 1.6089E8 |
| 524 | 1.6182E8 | 1.6182E8 | 1.6151E8 | 1.6150E8 |
| 525 | 1.6243E8 | 1.6243E8 | 1.6213E8 | 1.6212E8 |
| 526 | 1.6305E8 | 1.6305E8 | 1.6274E8 | 1.6274E8 |
| 527 | 1.6367E8 | 1.6367E8 | 1.6336E8 | 1.6336E8 |
| 528 | 1.6429E8 | 1.6429E8 | 1.6398E8 | 1.6398E8 |
| 529 | 1.6492E8 | 1.6492E8 | 1.6460E8 | 1.6460E8 |
| 530 | 1.6554E8 | 1.6554E8 | 1.6523E8 | 1.6522E8 |
| 531 | 1.6616E8 | 1.6616E8 | 1.6585E8 | 1.6585E8 |
| 532 | 1.6679E8 | 1.6679E8 | 1.6648E8 | 1.6647E8 |
| 533 | 1.6742E8 | 1.6742E8 | 1.6710E8 | 1.6710 E8 |
| 534 | 1.6805E8 | 1.6804E8 | 1.6773E8 | 1.6773 E8 |

| High Frequency Band | | | | |
|---|---|---|---|---|
| No. | F-F (A) | F-F (W) | P-P (A) | P-P (W) |
| 1005 | 5.9470E8 | 5.9469E8 | 5.9411E8 | 5.9409 E8 |
| 1006 | 5.9588E8 | 5.9588E8 | 5.9529E8 | 5.9527 E8 |
| 1007 | 5.9707E8 | 5.9706E8 | 5.9647E8 | 5.9646 E8 |
| 1008 | 5.9825E8 | 5.9825E8 | 5.9766E8 | 5.9764 E8 |
| 1009 | 5.9944E8 | 5.9944E8 | 5.9884E8 | 5.9883 E8 |
| 1010 | 6.0063E8 | 6.0062E8 | 6.0003E8 | 6.0002 E8 |
| 1011 | 6.0182E8 | 6.0181E8 | 6.0122E8 | 6.0121 E8 |
| 1012 | 6.0301E8 | 6.0300E8 | 6.0241E8 | 6.0240 E8 |
| 1013 | 6.0420E8 | 6.0420E8 | 6.0360E8 | 6.0359 E8 |
| 1014 | 6.0539E8 | 6.0539E8 | 6.0479E8 | 6.0478 E8 |
| 1015 | 6.0658E8 | 6.0658E8 | 6.0599E8 | 6.0597 E8 |
| 1016 | 6.0778E8 | 6.0778E8 | 6.0718E8 | 6.0717 E8 |
| 1017 | 6.0898E8 | 6.0897E8 | 6.0838E8 | 6.0836 E8 |
| 1018 | 6.1017E8 | 6.1017E8 | 6.0958E8 | 6.0956 E8 |
| 1019 | 6.1137E8 | 6.1137E8 | 6.1077E8 | 6.1076 E8 |
| 1020 | 6.1257E8 | 6.1257E8 | 6.1197E8 | 6.1196 E8 |
| 1021 | 6.1377E8 | 6.1377E8 | 6.1317E8 | 6.1316 E8 |
| 1022 | 6.1498E8 | 6.1497E8 | 6.1437E8 | 6.1436 E8 |
| 1023 | 6.1618E8 | 6.1618E8 | 6.1558E8 | 6.1556 E8 |
| 1024 | 6.1738E8 | 6.1738E8 | 6.1678E8 | 6.1677 E8 |
| 1025 | 6.1859E8 | 6.1859E8 | 6.1799E8 | 6.1797 E8 |
| 1026 | 6.1980E8 | 6.1979E8 | 6.1919E8 | 6.1918 E8 |
| 1027 | 6.2101E8 | 6.2100E8 | 6.2040E8 | 6.2038 E8 |
| 1028 | 6.2221E8 | 6.2221E8 | 6.2161E8 | 6.2159 E8 |
| 1029 | 6.2343E8 | 6.2342E8 | 6.2282E8 | 6.2280 E8 |
| 1030 | 6.2464E8 | 6.2463E8 | 6.2403E8 | 6.2401 E8 |
| 1031 | 6.2585E8 | 6.2585E8 | 6.2524E8 | 6.2523 E8 |
| 1032 | 6.2706E8 | 6.2706E8 | 6.2646E8 | 6.2644 E8 |
| 1033 | 6.2828E8 | 6.2828E8 | 6.2767E8 | 6.2766 E8 |
| 1034 | 6.2950E8 | 6.2949E8 | 6.2889E8 | 6.2887 E8 |